1-1-2010

# Parametric Analysis of a Coupled Photovoltaic/ Thermal Concentrating Solar Collector for Electricity Generation

Todd Otanicar
*Loyola Marymount University*, totanicar@lmu.edu

I. Chowdhury

P. E. Phelan

R. Prasher

# Parametric analysis of a coupled photovoltaic/thermal concentrating solar collector for electricity generation

Todd Otanicar,[1,a)] Ihtesham Chowdhury,[2] Patrick E. Phelan,[2] and Ravi Prasher[2]
[1]*Department of Mechanical Engineering, Loyola Marymount University, Los Angeles, California 90045, USA*
[2]*Mechanical and Aerospace Engineering, Arizona State University, Tempe, Arizona 85287, USA*

(Received 21 June 2010; accepted 15 October 2010; published online 9 December 2010)

The analysis of the combined efficiencies in a coupled photovoltaic (PV)/thermal concentrating solar collector are presented based on a coupled electrical/thermal model. The calculations take into account the drop in efficiency that accompanies the operation of PV cells at elevated temperatures along with a detailed analysis of the thermal system including losses. An iterative numerical scheme is described that involves a coupled electrothermal simulation of the solar energy conversion process. In the proposed configuration losses in the PV cell due to reduced efficiencies at elevated temperatures and the incident solar energy below the PV bandgap are both harnessed as heat. This thermal energy is then used to drive a thermodynamic power cycle. The simulations show that it is possible to optimize the overall efficiency of the system by variation in key factors such as the solar concentration factor, the band gap of the PV material, and the system thermal design configuration, leading to a maximum combined efficiency of ~32.3% for solar concentrations between 10–50 and a band-gap around 1.5–2.0 eV. © *2010 American Institute of Physics*. [doi:10.1063/1.3514590]

## I. INTRODUCTION

The possibility of enhancing the overall efficiency or utility of solar energy collection by creating a hybrid photovoltaic (PV)/thermal solar collector has been investigated by many authors[1–8] both analytically and numerically. However, most of the work in this area is at relatively low temperatures, with little or no solar concentration, in order to avoid the drops in efficiency associated with operation of PV cells at elevated temperatures.[3,9] In fact, the temperature-dependent efficiency drop has led to a significant amount of work dedicated to proper cooling of concentrated PV cells.[10] Furthermore the systems setting the record levels of cell efficiency under concentration are achieved with complex and expensive multi-junction tandem cells.[11] Some theoretical analyses of higher temperature hybrid collectors at high solar concentration factors have been reported in the literature[3–7] and there is also an experimental report of such a system operating at 65 °C.[8] Additionally the large amount of research into heat engines, particularly organic Rankine cycles, that utilize low temperature or waste heat energy sources[12,13] presents a renewed opportunity into analyzing such a concentrated hybrid system.

This work extends the concept of a hybrid PV/thermal system at high concentration ratios and temperatures by creating a coupled electrothermal model of the entire system. The goal is to optimize the overall efficiency of the system by examining the interplay of the PV efficiency with the solar thermal collector's operating parameters. We also take into account the dependence of the overall efficiency on the band-gap of the PV material to identify possible candidates for the hybrid system from the wide range of PV materials reported in the literature,[14] limited in this study to single-junction cells. This model goes beyond previous models by utilizing the detailed PV-temperature relationships developed in Refs. 15–17 applied to a concentrating system and coupling that to a detailed heat transfer model. Previous work has either utilized a simplified PV-temperature relationship or a simplified thermal model, not a combination of two coupled, relatively detailed, models. Additionally, a parametric approach is taken to understand the complex dynamics of the main design variables: concentration ratio, cell band-gap, and mass flow rate.

## II. MODELING

### A. Electrical model

The efficiency of the PV cell at a given temperature is calculated using a formulation presented in Refs. 15 and 16. This model is also similar to what was developed as part of the JOULE project PV-Hybrid-PAS as presented in Ref. 17, the main difference being the inclusion of concentrated solar irradiance and coupling to a detailed heat transfer model. The dark saturation current $J_{00}$ in the cell is given as

$$J_{00} = K' T^{3/n} \exp\left(\frac{-E_g}{mk_B T}\right), \tag{1}$$

where $K'$, $m$, and $n$ are empirical parameters, $T$ the temperature, $E_g$ the band-gap energy, and $k_B$ the Boltzmann constant. The short-circuit current $J_{sc}$ can be computed as[16]

$$J_{sc} = \int_{280}^{\lambda_g} eF(\lambda)d\lambda, \tag{2}$$

where $\lambda_g$ is the wavelength of solar radiation corresponding to the band-gap of the PV material, $e$ the electron charge, and $F$ the photon flux. The open-circuit voltage $V_{oc}$ is then calculated as:

[a)]Electronic mail: todd.otanicar@lmu.edu.

 

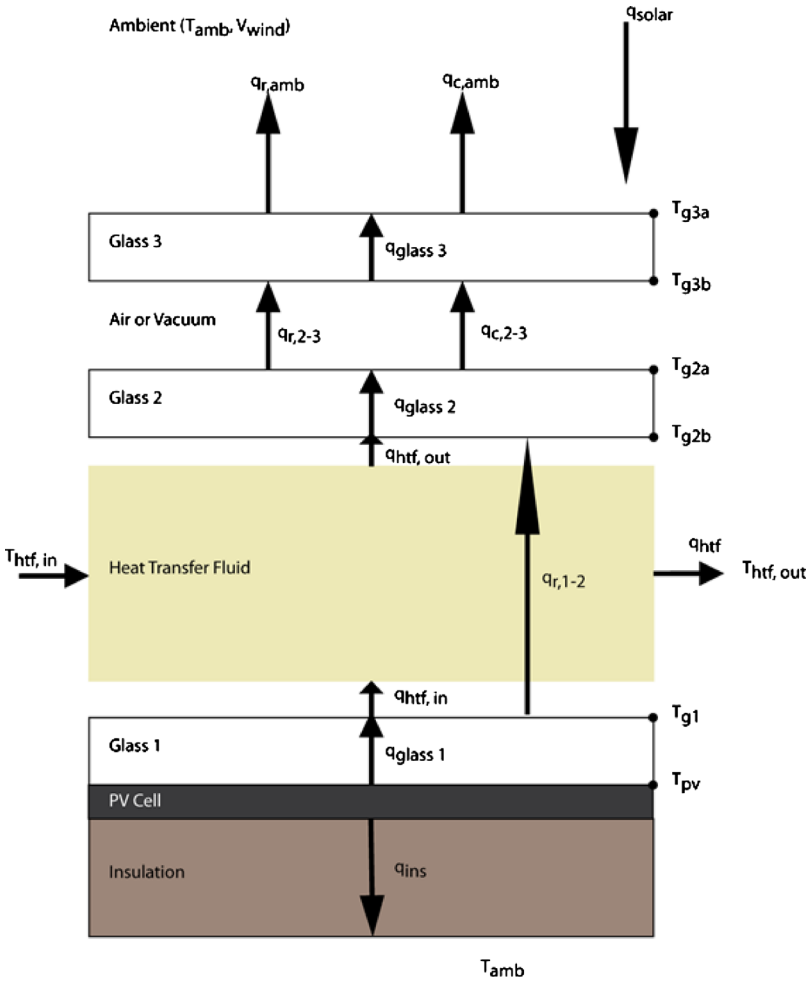


FIG. 1. (Color online) PV/thermal hybrid collector schematic for thermal modeling.

$$V_{oc} = \frac{Ak_BT}{e}\ln\left(\frac{CJ_{sc}}{J_{00}} + 1\right), \tag{3}$$

where $A$ is the diode factor and $C$ the concentration ratio. The fill-factor $FF$ is given by:

$$FF = \frac{V_m}{V_{oc}}\left[1 - \frac{\exp\left(\frac{eV_m}{k_BT}\right) - 1}{\exp\left(\frac{eV_{oc}}{k_BT}\right) - 1}\right]. \tag{4}$$

$V_m$ is the voltage at the maximum power point of the $I$-$V$ curve and is obtained from the relationship:

$$\exp\left(\frac{eV_m}{k_BT}\right)\left(1 + \frac{eV_m}{k_BT}\right) = \frac{CJ_{sc}}{J_{00}} + 1. \tag{5}$$

The final PV efficiency $\eta_{\mathrm{PV}}$ is then calculated as

$$\eta_{\mathrm{PV}} = \frac{V_{oc}J_{sc}FF}{CGA}, \tag{6}$$

where $G$ is the solar irradiance and $A$ is the system area. What is important to note is the dependence of $\eta_{\mathrm{PV}}$ on temperature. This requires an accurate thermal model to determine the cell temperature needed in Eqs. (1) and (3)–(5).

### B. Thermal model

In order to perform the thermal analysis a starting configuration for the collector must be assumed. For this model the collector design outlined in Fig. 1 was assumed. The first step in the solution procedure is to derive a set of equations representing the thermal energy balance for each surface:[18]

$$\tau_{sys}\alpha_{\mathrm{PV}}(1 - \eta_{\mathrm{PV}})CG = q_{ins} + q_{glass,1}, \tag{7}$$

$$q_{glass,1} = q_{\mathrm{HTF},in} + q_{r,1-2}, \tag{8}$$

$$q_{\mathrm{HTF},in} + \tau_{g3}\tau_{g2}\alpha_{\mathrm{HTF}}CG + \alpha_{\mathrm{HTF}}q_{r,1-2} = q_{\mathrm{HTF},out} + q_{\mathrm{HTF}}, \tag{9}$$

$$q_{\mathrm{HTF},out} + (1 - \alpha_{\mathrm{HTF}})q_{r,1-2} = q_{glass,2}, \tag{10}$$

$$q_{glass,2} = q_{r,2-3} + q_{c,2-3}, \tag{11}$$

$$q_{r,2-3} + q_{c,2-3} = q_{glass,3}, \tag{12}$$

$$q_{glass,3} = q_{r,amb} + q_{c,amb}, \tag{13}$$

where $\tau_{sys}$ is the transmittance of the combined glass-fluid system, $q$ the heat transfer rate per unit area where subscripts $r$ and $c$ are radiation and convection, respectively, $\alpha_{\mathrm{HTF}}$ is the solar-weighted absorptance of the heat transfer fluid (HTF),

$\alpha_{PV}$ is the absorptance of the PV cell, and $\tau_g$ is the transmittance of the glass.[19–23]

This results in seven equations for the energy balance and seven unknown temperatures within the system. As can be seen with Eq. (7) the overall energy balance relies on the PV efficiency requiring a coupled iterative approach with the PV modeling equations [Eqs. (1)–(6)]. Currently the model does not include the first-order reflection from the PV cell and glass surface 1 that would eventually be absorbed in the system. Future modeling efforts would include these more complex terms in the thermal model, although it is not expected to have a noticeable impact on the results. To start the thermal model iterations it helps to select initial values for all the temperatures; this is chosen initially with $T_{PV}$ being the greatest temperature and all temperatures being at least equal to the ambient temperature.

As can be seen, the energy balances are not explicitly related to the temperatures defined in Fig. 1. To complete the thermal model an expansive set of heat transfer equations is necessary to find a solution[18] and can be found in the supplemental information in Ref. 24. To determine the thermal efficiency $\eta_{th}$ (not the overall efficiency) the following relationship is used:

$$\eta_{th} = \frac{\dot{m} c_p (T_{out} - T_{in})}{CGA}, \tag{14}$$

where $T_{out}$ is the HTF outlet temperature, $T_{in}$ the HTF inlet temperature, and $\dot{m}$ the mass flow rate. The overall efficiency of the hybrid PV/thermal system $\eta_0$ is defined as:

$$\eta_0 = \eta_{PV} + \eta_{th} K \left(1 - \frac{T_{amb}}{T_{out}}\right), \tag{15}$$

where $T_{amb}$ is the ambient temperature and $K$ is the fraction of thermal energy converted to electrical output. This definition of overall efficiency provides a measure of the useful electrical power that is finally obtained. It is assumed that the fraction of the thermal energy that is converted into electrical output is a fraction, $K$, of the Carnot efficiency where the ideal Carnot cycle operates between the peak temperature of the fluid at the exit of the concentrating solar collector and the ambient temperature. The value of $K$ is assumed to be 0.5 in all the following calculations following previous studies[5] as it is representative of state-of-the-art thermal-electric conversion schemes. A detailed analysis of such systems is beyond the scope of this paper. Note that $K$ is equivalent to what is normally called the "second-law efficiency."

## III. RESULTS AND DISCUSSION

The coupled electrothermal model described above was solved using an Excel-based solver routine that performed iterations between the electrical and thermal equations. We selected the following values for the empirical parameters in this calculation following the discussion in Refs. 15 and 16: $K' = 0.05$, $m = 1.02$, $n = 0.98$, and $A = 1$. Additional parameters required by the model are detailed in Table I. Using these values, we found good agreement with PV cell efficiencies reported in the literature. For example, at 25 °C and no solar concentration, our model predicts PV efficiencies of 24.25% and 26.53% for Si and GaAs cells, respectively. This is comparable to the values reported in the literature of $24.7 \pm 0.5\%$ for Si and $25.1 \pm 0.8\%$ for GaAs.[25] We compared this model's predictions with the measured values from Ref. 8 which reported a drop in efficiency of ~3.2% in a Si cell when elevated to 65 °C. Our model predicts a similar decrease (~3.7%) for Si in going from 25 to 65 °C. For the variation with the solar concentration factor, we calculated the efficiency of a Si cell to be 29.27% at 96 suns and 25 °C. This is comparable to the value of $26.8 \pm 0.8\%$ reported in Ref. 25 for the same conditions. All these calculations were performed using the direct+circumsolar AM1.5 spectrum values obtained from Refs. 26.

TABLE I. Thermal properties used in modeling.

| Property | Value | Refs. |
|---|---|---|
| Solar flux | 1000 $W/m^2$ | 19 |
| PV absorbance (solar band) | 0.8 | 20 |
| Glass transmittance (solar band) | 0.9 | 20 |
| Glass emittance (thermal band) | 0.9 | 20 |
| HTF absorbance (solar band) | 0.021 | 21 |
| HTF thermal conductivity | 0.085 W/m K | 22 |
| HTF specific heat | 2478 J/kg K | 22 |
| Glass thermal conductivity | 0.8 W/m K | 23 |

The overall variation in the PV efficiency in the coupled model with the band-gap and solar concentration factor is shown in Fig. 2. Figure 3 demonstrates the rapid decrease in the PV cell efficiency as the PV cell temperature increases under increasing levels of concentration. It is to be noted that the PV efficiency was calculated at the mean temperature, not the peak, as there is a temperature gradient along the direction of flow. This nonuniformity in temperature can lead to a reduction in the PV current as has been discussed in the literature.[25] We do not take this effect into account in our model currently. It is seen from Fig. 2 that the PV efficiency peaks around a band gap of 1.5–2 eV and that there is a gradual reduction and shift to higher band-gaps as the solar concentration factor is increased. This is expected as the PV temperature also increases with the increase in the solar concentration as seen from Fig. 3. Interestingly in Fig. 3 the efficiency curve for band-gap 1.5 eV drops below that of 2.5 eV demonstrating the necessity for large parameter sweeps and optimizations depending on concentration ratios, materials and system geometry.

The thermal efficiency variation is shown in Fig. 4. The thermal efficiency shows a dip at the intermediate band-gaps corresponding to the high PV efficiency region. This demonstrates the coupled nature of the problem as increased absorption in the PV cell necessarily reduces the fraction of energy that can be absorbed thermally. Also, there is a reduction in thermal efficiency as the solar concentration increases even though the peak HTF temperature goes up due to the increased radiative losses at the higher temperatures.

The overall efficiency calculated from Eq. (15) is plotted in Fig. 5. It is seen that the overall efficiency reaches a maximum over a region that roughly corresponds to solar concentrations between 10–50 and a band-gap around 1.5–2.0 eV.

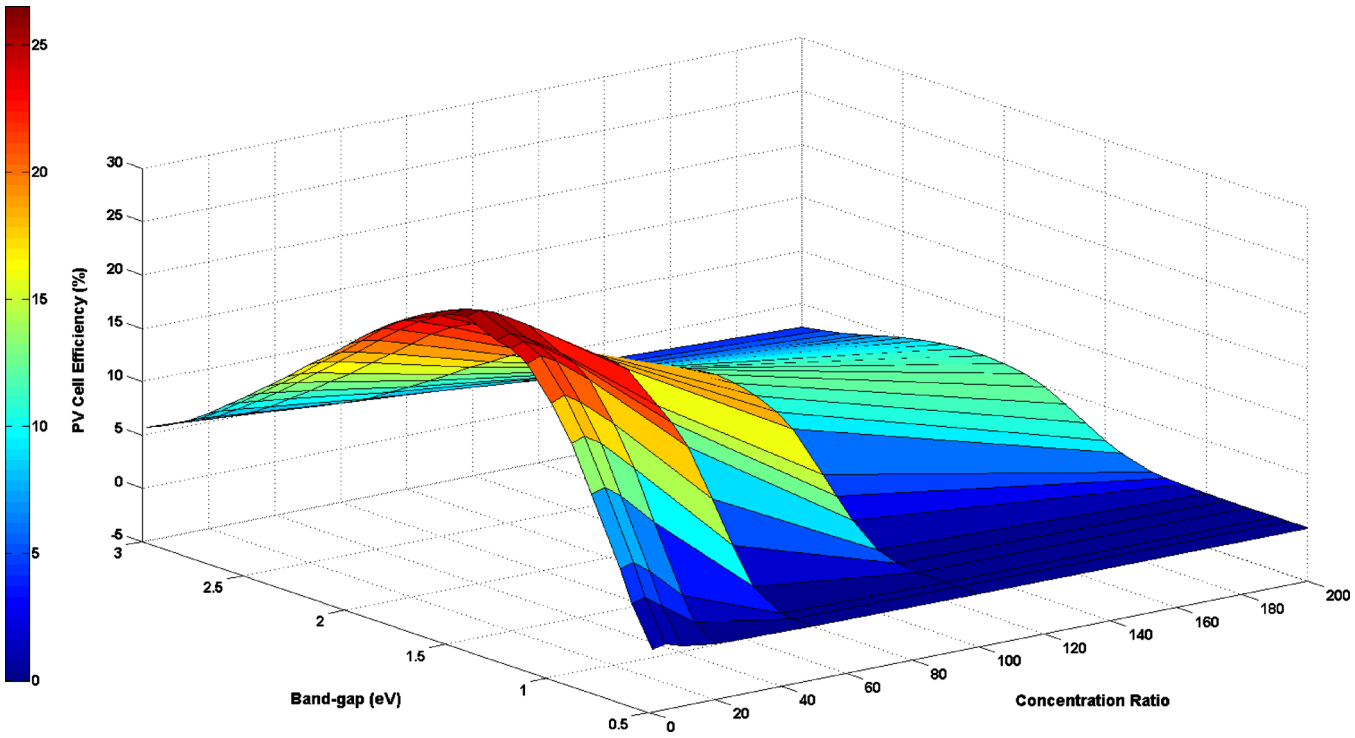


FIG. 2. (Color online) PV efficiency variation with band-gap and solar concentration ($\dot{m}$=0.05 kg/s).

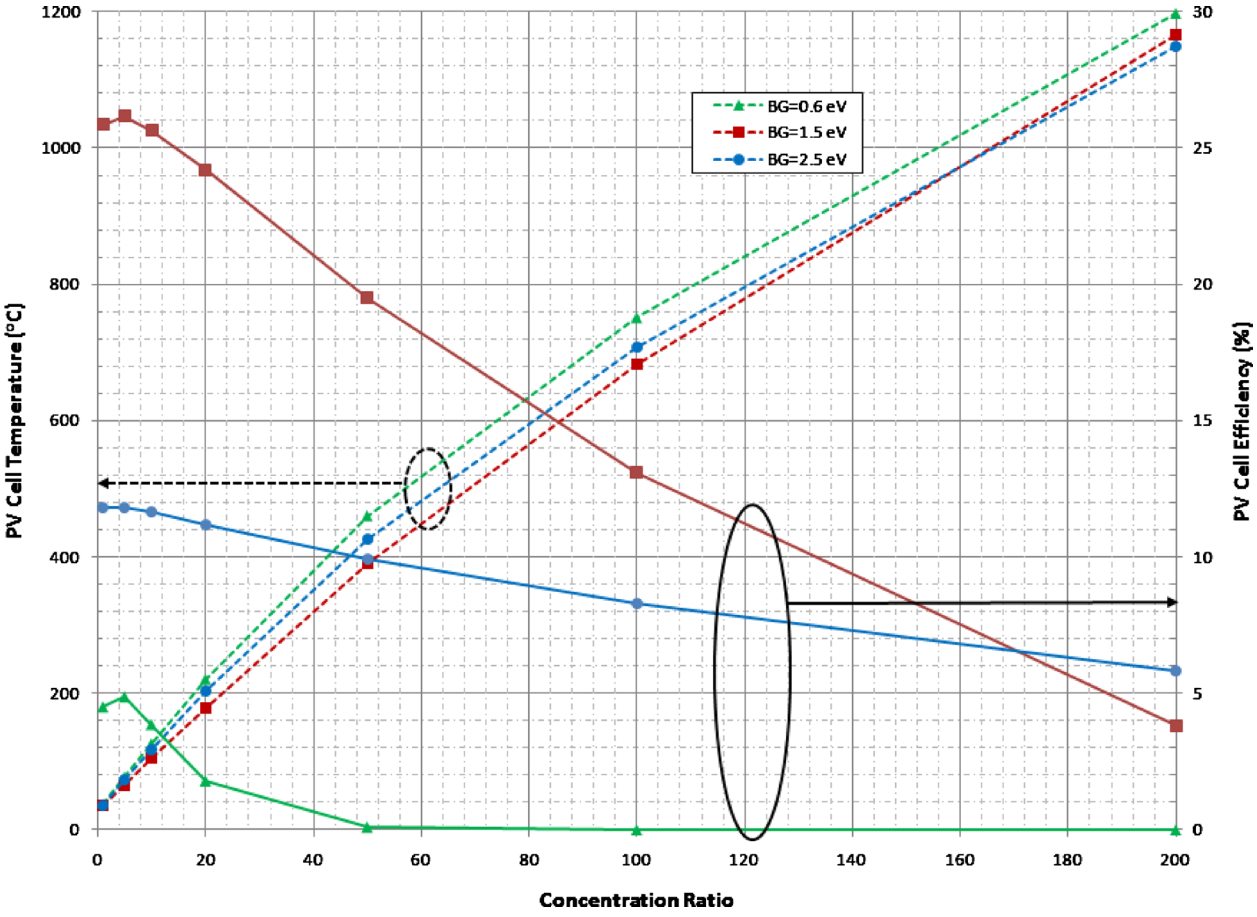


FIG. 3. (Color online) PV cell peak temperature (in degree Celsius) at the exit of the collector ($\dot{m}$=0.05 kg/s).

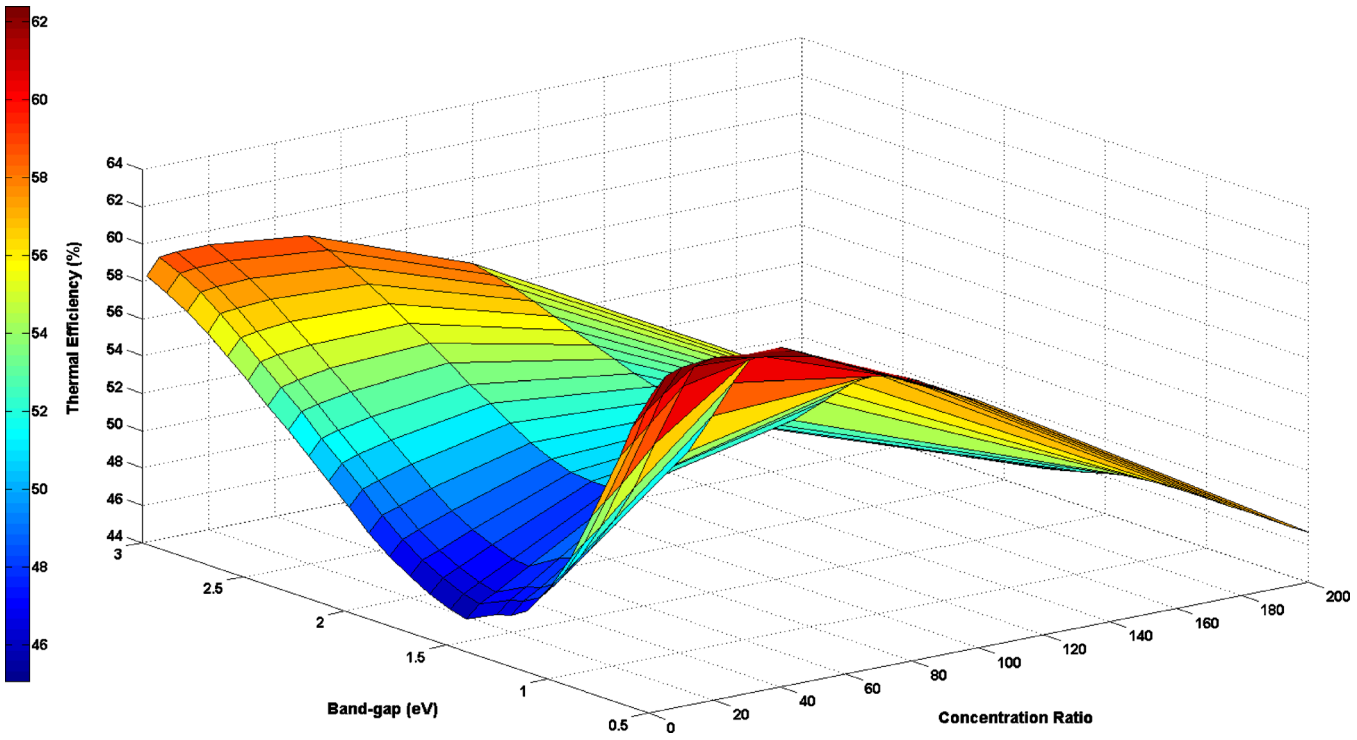


FIG. 4. (Color online) Thermal efficiency variation with band-gap and solar concentration factor ($\dot{m}$=0.05 kg/s).

The maximum efficiency value that we have calculated, at a mass flow rate of 0.05 kg/s, is ~30.3% with the PV contributing about 24% (in absolute terms) at this point. The mean PV temperature in this regime is ~100 °C. The thermal efficiencies can definitely go up with better control over the thermal losses which are a function of the thermal design. The peak fluid temperature is about 250 °C which opens up the potential for operating at much lower temperatures than conventional concentrating solar power collectors, typically between 350 and 750 °C depending on the configuration[27,28] that would bring significant cost benefits for the thermal-electric conversion scheme. Figure 6 presents the ratio of the PV efficiency ($\eta_{PV}$) to the overall efficiency ($\eta_0$). For the configuration studied in this paper, the PV contributes most

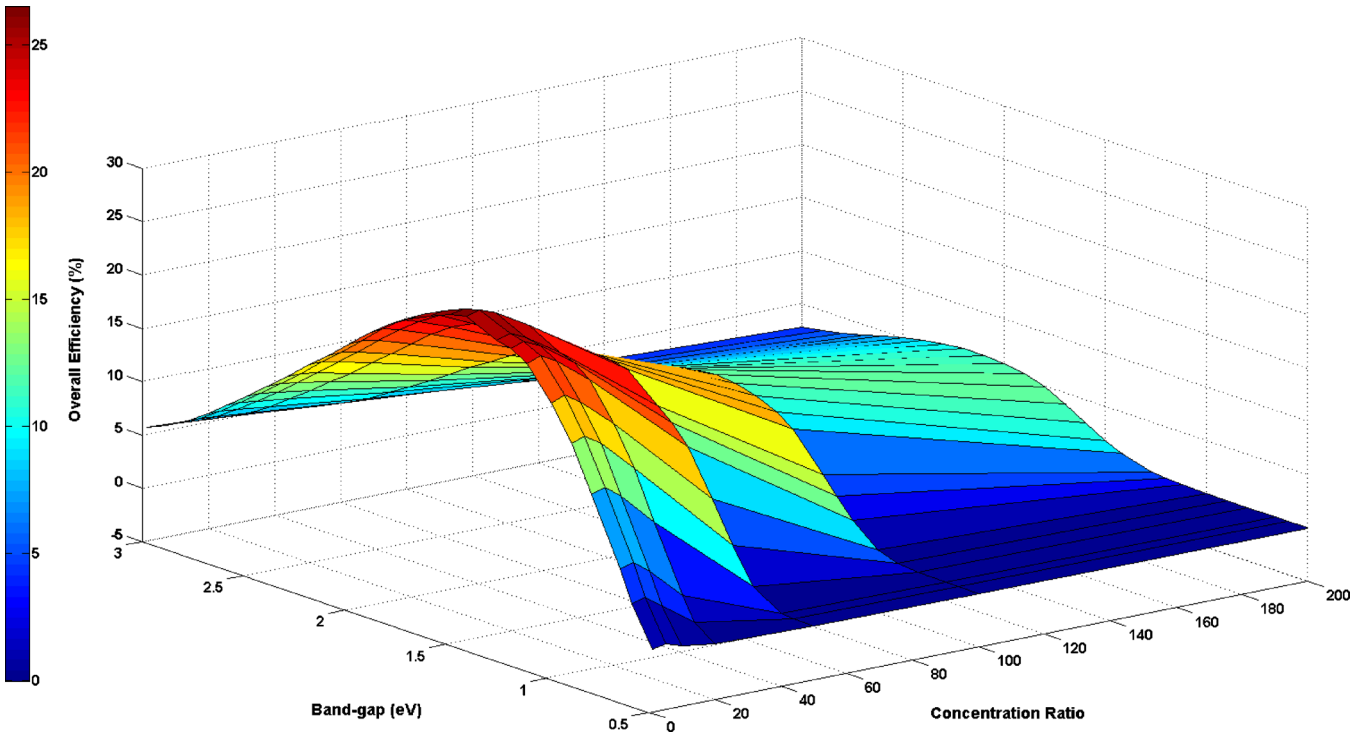


FIG. 5. (Color online) Overall efficiency variation with band-gap and solar concentration ($\dot{m}$=0.05 kg/s).

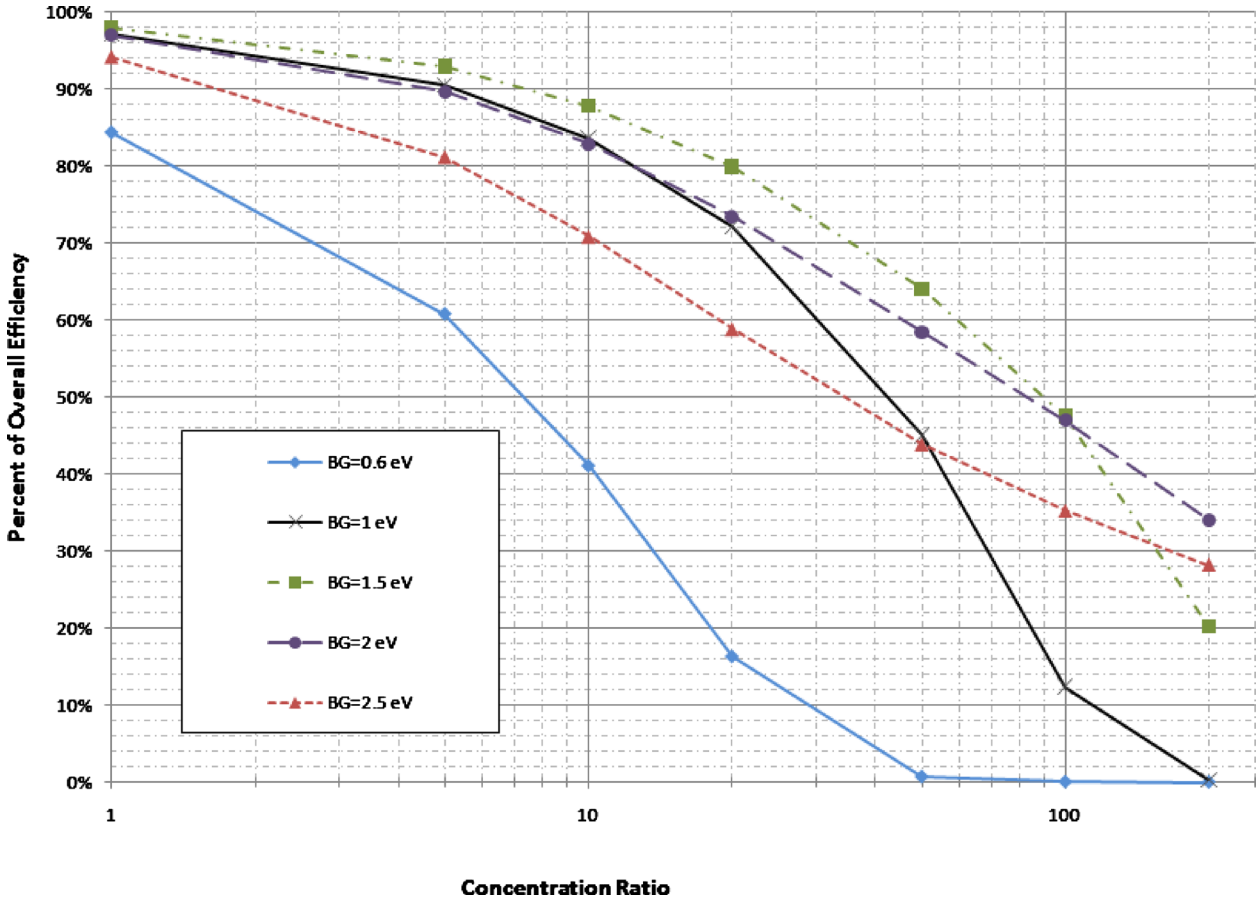


FIG. 6. (Color online) Fraction of overall efficiency contributed by the PV cell ($\dot{m}$=0.05 kg/s).

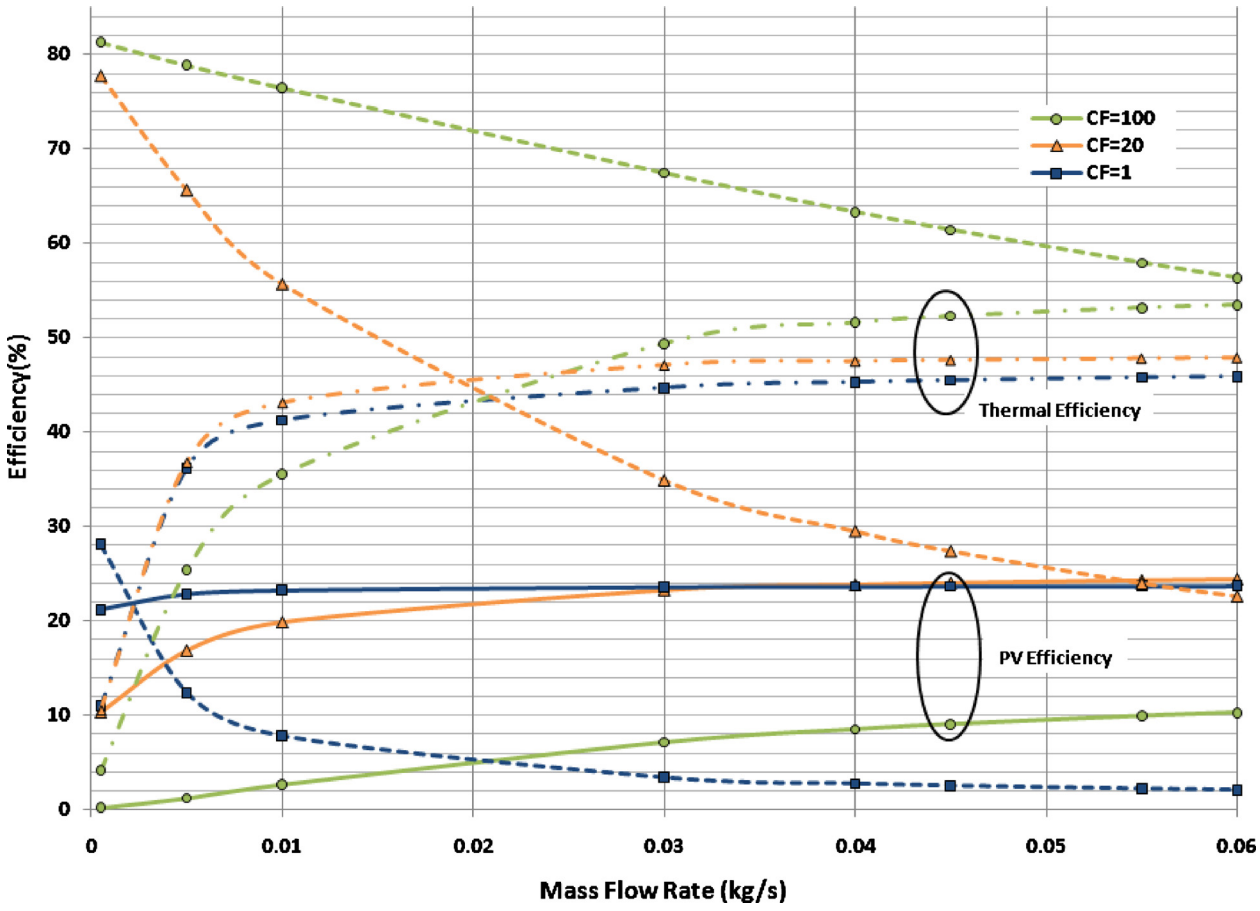


FIG. 7. (Color online) Mass flow rate effects on PV (solid), thermal (dashed-dotted), and Carnot (dashed) efficiency for a selected band-gap of 1.42 eV.

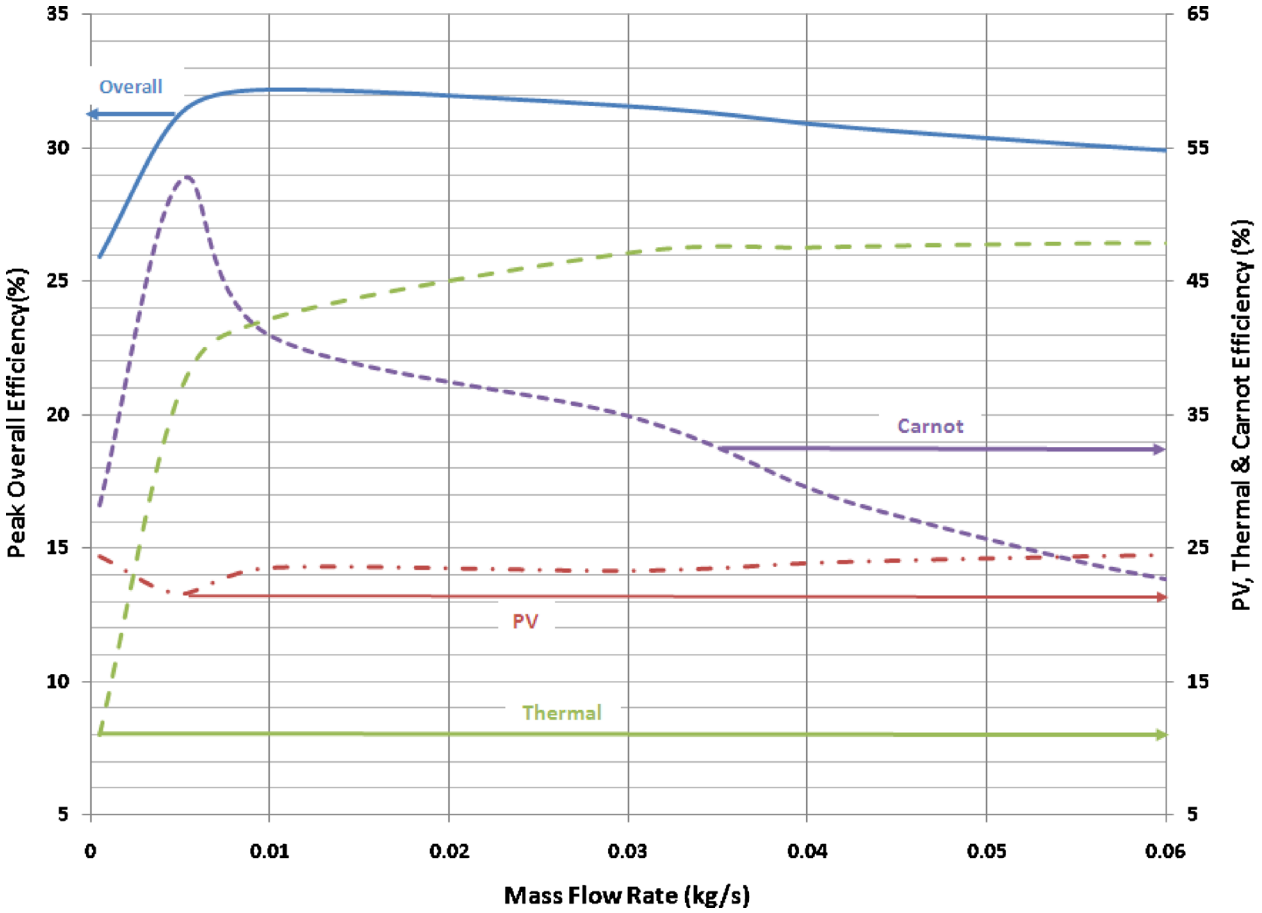


FIG. 8. (Color online) Impact of mass flow rate on the maximum overall efficiency, and corresponding thermal, Carnot, and PV efficiency observed in the design space.

of the efficiency at low concentration ratios with a significant falloff as the ratio is increased. The contributions from the thermal system versus the PV cell are also highly dependent on the choice of mass flow rate.

To demonstrate the complex impact of the mass flow rate on the operating efficiency of the modeled system the results of the PV, thermal, and Carnot efficiency for a PV cell with band-gap of 1.42 eV under different flow rate and concentration factors is shown in Fig. 7. The impact of mass flow rate to the PV efficiency is greatest at the largest concentration ratios due to the strong dependence on PV cell temperature and mass flow rate. Similarly increased mass flow rate has an initial rapid increase on the thermal efficiency which asymptotically levels off at the higher levels of flow rate. The rapid increase and asymptotic leveling can be attributed to the competing terms in Eq. (14), the mass flow rate and HTF inlet-to-outlet temperature difference. The variation in Carnot efficiency demonstrates the impact the mass flow rate has on the outlet HT temperature, decreases as the mass flow rate increases, as well as the demonstration that at higher concentration factors this temperature decrease is affected less by increasing mass flow rate.

All of these impacts combine to affect the peak overall efficiency calculated for a given mass flow rate with band-gap and concentration ratio still varying as shown in Fig. 8. It should be noted that plot shows the maximum overall efficiency, along with the corresponding PV, thermal, and Carnot efficiencies at the maximum overall efficiency point, across the range of band-gaps and concentration ratios considered. As seen in Fig. 8 there is a rapid increase in overall efficiency with mass flow rate until a maximum value at a mass flow rate of 0.01 kg/s followed by a slow decrease in overall efficiency. A couple of interesting results are demonstrated within this figure: the optimal overall system does not continually increase with flow rate, and since the PV, thermal, and Carnot efficiencies corresponding to the point of maximum overall efficiency are plotted (not the maximum efficiency values for each parameter) it can be seen that the maximum overall efficiency is simply not just a case of maximizing one system but balancing both systems. These dynamic effects lead to a challenging optimization problem since the combined effects vary across band-gap, concentration ratio, and mass flow rate. For instance the low mass flow rate conditions produce optimal overall efficiencies at low concentration levels while increased mass flow rate leads to an optimal overall efficiency at higher concentrations. These results also demonstrate the complex nature of determining the peak overall efficiency and the need for a coupled model that can quickly search across a large design space as demonstrated here.

From the materials viewpoint, there have been reports in the literature recently looking at PV materials from the standpoint of availability and extraction cost as well as efficiency and thus identifying materials that may have signifi-

cant potential. Out of the materials highlighted in Ref. 14, three potential candidates—$Zn_3P_2$, CuO, and $Cu_2O$—stand out as being suitable for a hybrid PV/thermal collector operating at high temperatures. These materials have bandgaps of 1.55 eV, 1.3 eV, and 2.0 eV, respectively,[29,30] which fall in the regime of interest according to the results shown in Fig. 6. Thus, looking at materials other than the conventional GaAs and Si cells may prove to be valuable for this particular application and may provide a highly cost-effective solution.

## IV. CONCLUSION

We have created a coupled electrothermal model of a hybrid PV/thermal concentrating solar collector that enables a detailed analysis of the interaction between the temperature-dependent PV efficiency and the design parameters of the thermal collector. The preliminary results suggest that this hybrid system can achieve competitive efficiency values through careful thermal design and selection of PV materials. Additionally the system operates with a very simple PV configuration compared to other concentrating PV systems. Based on the results significant opportunities for further efficiency enhancements exist through different thermal design configurations which can lessen the thermal coupling between the PV cell and thermal working fluid. One approach to this is to change the absorptivity of the HTF, resulting in an increase in the thermal fluid temperature while reducing the PV cell temperature. This is an optimization exercise that will be carried out in the future as this coupled electrothermal model is extended.

[1]T. T. Chow, Appl. Energy **87**, 365 (2010).
[2]B. Singh and M. Y. Othman, J. Renewable Sustainable Energy **1**, 062702 (2009).
[3]H. J. Hovel, Sol. Energy **19**, 605 (1977).
[4]D. J. Mbewe, H. C. Card, and D. C. Card, Sol. Energy **35**, 247 (1985).
[5]Y. V. Vorobiev, J. González-Hernández, and A. Kribus, ASME J. Sol. Energy Eng. **128**, 258 (2006).
[6]Yu. Vorobiev, J. González-Hernández, P. Vorobiev, and L. Bulat, Sol. Energy **80**, 170 (2006).
[7]G. Mittelman, A. Kribus, and A. Dayan, Energy Convers. Manage. **48**, 2481 (2007).
[8]J. S. Coventry, Sol. Energy **78**, 211 (2005).
[9]D. Meneses-Rodríguez, P. P. Horley, J. Gonzalez-Hernandez, Y. V. Vorobiev, and P. N. Gorley, Sol. Energy **78**, 243 (2005).
[10]A. Royne, C. J. Dey, and D. R. Mills, Sol. Energy Mater. Sol. Cells **86**, 451 (2005).
[11]M. Yamaguchi, T. Takamoto, and K. Araki, Sol. Energy Mater. Sol. Cells **90**, 3068 (2006).
[12]B. F. Tchanche, G. Papadikis, G. Lambrinos, and A. Frangoudakis, Appl. Therm. Eng. **29**, 2468 (2009).
[13]X. Shi and D. Che, Energy Convers. Manage. **50**, 567 (2009).
[14]C. Wadia, A. P. Alivisatos, and D. M. Kammen, Environ. Sci. Technol. **43**, 2072 (2009).
[15]J. C. C. Fan, Sol. Cells **17**, 309 (1986).
[16]J. C. C. Fan, B.-Y. Tsaur, and B. J. Palm, Proc. SPIE **407**, 73 (1983).
[17]T.-T. Chow, Sol. Energy Mater. Sol. Cells **93**, 230 (2009).
[18]H. A. Zondag, D. W. de Vries, W. G. J. van Helden, R. J. C. van Zolingen, and A. A. van Steenhoven, Sol. Energy **74**, 253 (2003).
[19]J. A. Duffie and W. A. Beckman, *Solar Engineering of Thermal Processes* (Wiley, New York, 1980).
[20]J. I. Rosell, X. Vallverdú, M. A. Lechón, and M. Ibáñez, Energy Convers. Manage. **46**, 3034 (2005).
[21]T. P. Otanicar, P. E. Phelan, and J. S. Golden, Sol. Energy **83**, 969 (2009).
[22]Solutia (1998), Therminol VP-1 Vapor Phase Liquid Phase Heat Transfer Fluid Bulletin.
[23]Y. A. Cengel, *Heat Transfer: A Practical Approach* (McGraw Hill, NY, 2003).
[24]See supplementary material at http://dx.doi.org/10.1063/1.3514590 for supplementary detailed heat transfer infromation.
[25]M. A. Green, K. Emery, D. L. King, Y. Hisikawa, and W. Warta, Prog. Photovoltaics **14**, 45 (2006).
[26]http://rredc.nrel.gov/solar/spectra/am1.5/
[27]A. Luque, G. Sala, and J. C. Arboiro, Sol. Energy Mater. Sol. Cells **51**, 269 (1998).
[28]D. Mills, Sol. Energy **76**, 19 (2004).
[29]A. M. Hermann, A. Madan, M. W. Wanlass, V. Badri, R. Ahrenkiel, S. Morrison, and C. Gonzales, Sol. Energy Mater. Sol. Cells **82**, 241 (2004).
[30]N. Serin, T. Serin, S. Horzum, and Y. Celik, Semicond. Sci. Technol. **20**, 398 (2005).